Chapter 3

Materials and Experimental Techniques

Abstract

This chapter is focused on the materials and methodology used for studying metal hydrides. Main focus is on high energy ball milling for synthesis of the alloy compositions. Also, high-lights are presented on characterization techniques, namely tools for morphological, elemental analysis, quantitative analysis and structural analysis. The instrumentation used includes JEOL make scanning electron microscope (SEM) with attached energy dispersive X–ray spectrometer (EDS) and Bruker make X–ray diffractometer (XRD). Detail of the Sievert's apparatus is presented to studying hydriding–dehydriding characterization of the synthesized alloy compositions. In the end, thermal analysis is conducted using differential scanning calorimetry (DSC), which is also discussed (for measuring the enthalpy and entropy of formation of the developed alloy compositions).

3.1 Materials

The chemicals used and the sources from which they were obtained, are as follows:

The Magnesium (Mg) powder was purchased from Sisco Research Laboratories (SRL), Mumbai with particle size 36 mesh and minimum 99.8% purity. Similarly, Nickel (Ni) and Iron (Fe) metal powders were obtained from SRL with particle size 100 mesh and minimum 99.5% purity. Micro–Vanadium (V), Zirconium (Zr) and Manganese (Mn) were purchased from SUNC international, China, which has minimum 99% purity. The granular Palladium (Pd) powder was obtained from Oxford Laboratory Reagent, Mumbai with purity 99.999%. The Titanium (Ti) was purchased from ACROS Organics, US with minimum 99.5 % purity and particle size 100 mesh.

The organic materials were also used for the synthesis of the materials during wet milling process and cleaning purpose (petroleum ether, acetone, etc…). These were purchased from S D Fine – Chem Limited, Mumbai having minimum purity 95.0 % (Grade–LR). Hydrogen, having minimum 99.99 % purity with Grade–I was used for absorption/desorption experiments. It was purchased from URMI Enterprises, Vadodara, India.

3.2 Sample Preparation using High Energy Ball Milling Method

The planetary ball mill owes its name to the planet–like movement of its bowls [1]. Since the bowls and the supporting disc rotate in opposite directions, the centrifugal forces alternatively act in like and opposite directions. The enhancement of the forces acting on the balls in relation to the conventional ball mill is achieved by the combined action of two centrifugal fields. The charge inside bowls performs two relative motions: (i) a rotary motion around the mill axis and, (ii) a planetary motion around the bowl axis (see Fig. 3.1) [2]. This causes the milling balls to run down the inside wall of the bowls – the friction effect, followed by the material being milled. The milling balls are lifting by it and travelling freely through the inner chamber of the bowls and colliding against the opposite inside wall [3].

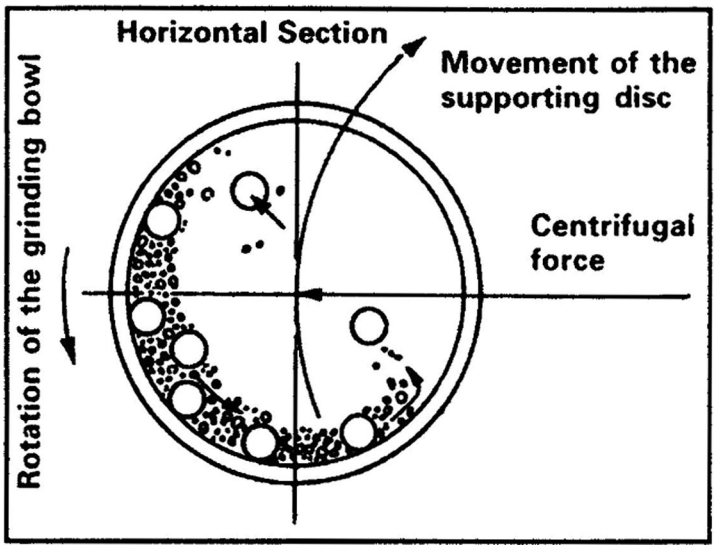

Fig. 3.1 Movements of working parts and balls in a planetary ball mill

3.2.1 Laboratory Planetary Ball Mill

The milling experiments are conducted in a planetary ball mill (see Fig. 3.2). The mill is driven by a squirrel cage induction motor with a power rating of 1 HP. The planetary mill, which has an available bowl volume of 250 cm^3 is controlled by a PLC (programmable logic control) drive, which enables bowl as well as plate speed variation from 45 to 500 RPM.

Fig. 3.2: Photographs showing planetary ball mill: (a) Front view and (b) Top view

.

The running and off time are fed into the range 0 to 255 minutes. Similarly, acceleration and deceleration time are fed into the range 0 to 10 seconds. All experiments are conducted in the wet milling mode. Petroleum ether is used as the process control agent (PCA). A charge to ball ratio of 1:10 is used. Hardened steel balls of 19 mm diameter are used as the grinding media.

3.2.2 Procedure of Ball Milling

For the synthesis of the alloys/compositions, using high energy planetary ball mill, the following steps are followed:

- ☼ Take out the bowls from “planetary ball milling”.
- ☼ Open the bowls and clean inner surface of bowls and steel balls using an appropriate organic solvent (petroleum ether, acetone, etc…), and water.
- ☼ Carefully weight each elemental species of the powder using “weighing balance”.
- ☼ The total mass of elemental powders should be generally taken 20 gm.
- ☼ Carefully transfer the weighted elemental powders in one bowl of the planetary ball mill.
- ☼ Add grinding media (in the form of steel balls) to the bowl, having the mass ratio of 1:10 (the cumulative ball mass should be 10 times the powder mass).
- ☼ Add process control agent (petroleum ether) having the ratio 2:1 with respect to the charge materials.
- ☼ Repeat same for bowl number–2.
- ☼ If the second bowl is not to be used for processing of material ensure that the machine is statically balanced by adding dummy mass (balls/shot charge) equivalent to the total mass added to the bowl number–1.
- ☼ Finally, the machine “operational parameters” are set. The plate and bowl speed are fixed at 350 RPM and 490 RPM, respectively. “Run” and “Off” time of ball milling are kept 10 minutes. Acceleration and deceleration time are kept 8 seconds.
- ☼ Number of cycle is varied as per milling time (One cycle is equal to “Run time” plus “Off time”. Hence, the one cycle is equal to 20 minutes, and it implies that an hour is equal to 3 cycles. Therefore, 40 h milling time, ball mill is required to complete 120 cycles).

3.3 Characterization Techniques

3.3.1 Scanning Electron Microscopy (SEM)

The scanning electron microscopy (SEM) is a type of electron microscope that creates images by focusing a high energy beam of electrons onto the surface of a sample and detecting signals from the interaction of the incident electrons with the sample's surface (see Fig. 3.3) [4–6]. SEM is generating two types of signals by electrons, namely, secondary electrons, and back scattered electrons. In the most common detection mode secondary electrons are used for imaging. Back scattered electrons are beam electrons that are reflected from the sample [7, 8].

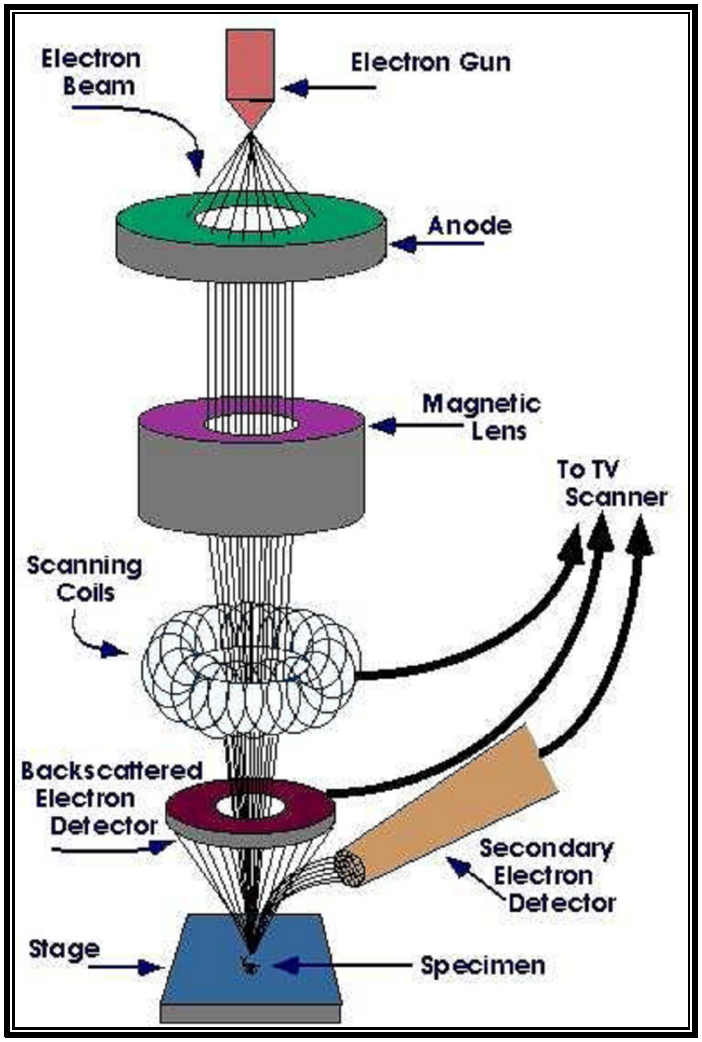

Fig. 3.3: Schematic view of a scanning electron microscopy (SEM)

The “electron source” at the top represents the electron gun, producing a stream of electrons. The stream is condensed by the first condenser lens (usually known as anode). This lens is used to both form the beam and limit the amount of current in the beam. It works in conjunction with the condenser aperture to eliminate the high angle electrons from the beam.

The beam is then constricted by the condenser aperture, eliminating some high angle electrons (generally, used magnetic lens). The second condenser lens forms the electrons into a thin, tight, coherent beam and is usually controlled by the “fine probe current knob”. A user selectable objective aperture further eliminates high angle electrons from the beam.

A set of coils then “scan” the beam in a grid fashion (like a television), consisting on points for a period of time determined by the scan speed (usually in the microsecond range). The final lens (the objective) focuses the scanning beam onto the part of the specimen desired. When the beam strikes the sample (and consists for a few microseconds) interactions occur inside the sample and are detected by detector. Before, the beam moves to its next point this detector count the number of electron interactions and display a pixel on a CRT (cathode ray tube), whose intensity is determined by this number (the more reactions the brighter the pixel). This process is repeated until the grid scan is finished and then repeated.

Laboratory SEM

The morphology of synthesized material is monitored by a JEOL make Scanning Electron Microscopy, model number JSM 6380LV (see Fig. 3.4). The working distance (WD, sample distance from objective lens) is varied from 15 mm to 20 mm as per resolution of the images. Same purpose, the spot size is also varied from 30 to 60. The accelerating voltage is fixed at 20 kV and filament current is kept nearly 85 μA to 100 μA to conduct morphological analysis. Inside the SEM chamber, the vacuum is created less than 10^{-7} torrs (within 5 minutes) for the minimizing impurities and viewing the sharp surfaces of the sample. The magnifications of the images are varied as per the image clarity. All micrographs are viewed into two

electron images mode: (a) Secondary Electron Image (SEI), and (b) Backscattered Electron Image (BEI).

Fig. 3.4: Photograph of the laboratory SEM

3.3.2 Energy Dispersive X–Ray Spectroscopy (EDS)

Energy dispersive X–ray spectroscopy (EDS) is an analytical technique used for the chemical elemental analysis of the samples. Its characterization capabilities are due in large part to the fundamental principle that each element has a unique atomic structure allowing X–rays that are characteristic of an element's atomic structure to be identified uniquely from one another [9, 10]. To stimulate the emission of characteristic X–rays from a specimen, a high energy beam of charged particles such as electrons or protons, or a beam of X–rays, is focused into the sample being studied. At rest, an atom within the sample contains ground state (or unexcited) electrons in discrete energy levels or electron shells bound to the nucleus. The incident beam may excite an electron in an inner shell, ejecting it from the shell while creating an electron hole where the electron was (see Fig. 3.5) [11]. An electron from an outer, higher energy shell then fills the hole, and the difference in energy between the higher

energy shell and the lower energy shell may be released in the form of an X–ray. The number and energy of the X–rays emitted from a specimen can be measured by an energy dispersive spectrometer. As the energy of the X–rays is characteristic of the difference in energy between the two shells, and of the atomic structure of the element from which they are emitted. This allows the elemental compositions of the specimen to be measured.

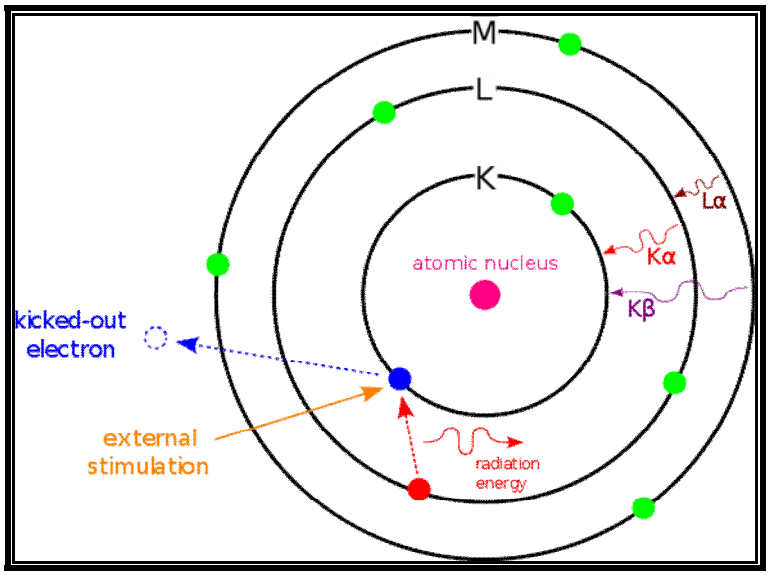

Fig. 3.5: Basic principle of the EDS

Laboratory EDS

The chemical elemental analysis of the synthesized material is studied by energy dispersive X–ray spectrometer (EDS) with attached SEM (JSM 6380LV) (see Fig. 3.4). This analysis is studied only secondary electron image (SEI) mode. The working distance, WD is kept 15 mm and spot size is kept 60. The accelerating voltage is fixed at 20 kV and filament current is kept nearly 85 μA to 100 μA to conduct this analysis. The process time to the acquisition spectrum is selected 70 second and dead time (during this period pulses are not measured) is selected 30% to maximize output. The cooling system is performed using liquid Nitrogen for this analysis.

3.3.3 X – Ray Diffractometer (XRD)

The XRD works on the principle of the diffraction. Diffraction is a special case of the interaction of a wave with matter [12, 13]. Diffraction in crystalline materials arises, when waves are scattered from atoms at different positions in the sample. The difference in path length will result in a phase shift between the waves, and superposition of the waves will result in differences in the detected intensity. The measured intensities can therefore give information about the relative positions of the atoms. Diffraction only occurs if the wavelength of radiation used is of the order of the separation distance of the scattering centres. X–rays have a wavelength, which is comparable to atomic separations and so makes them an ideal probe for crystalline materials [14].

The Bragg Equation

Treatment of diffraction as the reflection of X–rays by equally spaced lattice planes gives rise to the Bragg equation. If two X–rays (X_1 and X_2 in Fig. 3.6) are scattered from consecutive planes, the second wave travels a longer distance (from C to B before reflection and from B to D after reflection). Applying simple trigonometry to the geometrical arrangement shown in Fig. 3.6 gives the path difference (Δ) in terms of the plane separation (d) and the incident angle of the radiation (θ) [15]:

$$\Delta = (CB + BD) = (d\sin\theta + d\sin\theta) = 2d\sin\theta \qquad \text{---------- (3.1)}$$

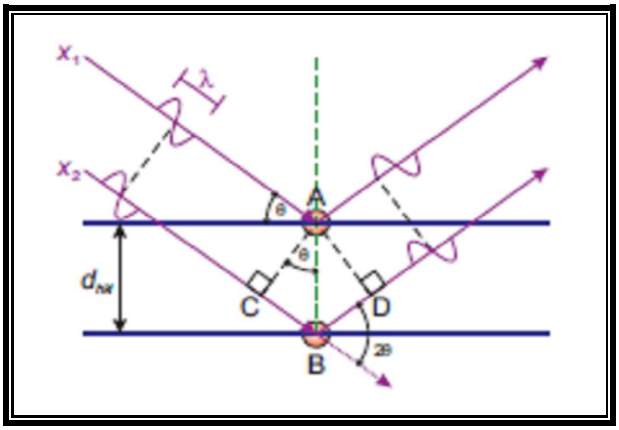

Fig. 3.6: The geometry used for simplified derivation of Bragg's law

Superposition resulting in constructive interference only occurs, if the path difference is equal to a multiple of the wavelength (the waves return to being in phase):

$\Delta = n\lambda$ ---------- (3.2)

Where, n is the 0, ±1, ±2, …….

Complete destructive interference results from all non integer values of n. Combining Eqns. 3.1 and 3.2 gives the Bragg equation [16, 17]:

$\therefore\ n\lambda = 2d \sin\theta$ ---------- (3.3)

In reality, X–rays are strongly penetrating and scattering can occur at thousands of consecutive planes in a single crystallite. Also, X–rays are scattered by the electron cloud of constituent atoms, not by the crystal planes. It is worth clarifying at this point how the Bragg equation is applied in a diffraction experiment. A single wavelength impinges onto the sample at a defined angle, θ. The intensity of scattered radiation at an angle 2θ is measured. Angles corresponding to the d–spacing of a lattice plane via the Bragg equation are said to obey Bragg's law and may have a significant diffracted intensity. The Bragg law still holds even if scattering occurs from atoms located at different positions within the lattice plane [18]. X–ray diffraction (XRD) experiment consists of a monochromatic source of radiation, which shines onto the sample and a detector, which is positioned in a defined geometry relative to the source and sample (see Fig. 3.7) [19].

Laboratory XRD

Laboratory powder XRD data are collected on a Bruker AXS D8 ADVANCE X–ray diffractrometer in reflection (Bragg-Brentano) geometry (see Fig. 3.7). A copper X–ray source is monochromated using a Germanium monochromator to give Cu – K_α radiation at a wavelength of 1.54056 ´. For minimizing K_β radiation, Ni filter is used. The accelerating voltage and current are kept fixed at 40 kV and 40 mA, respectively. The X – ray scanning range is fed into the 5° to 90° (2θ). The scanning speed is kept

0.025° per second. The experimental data is store as row file and it was evaluated by using DIFFRACT PLUS EVA software. The presence of the phases into the synthesized materials is identified by comparing experimental XRD patterns with standard ICDD (International Centre for Diffraction Data) cards.

Fig. 3.7: Photograph of the XRD

Peak profile shapes have a number of contributions, some from the instrumental factors such as the radiation source being used, instrument characteristics and set-up, and some from the sample such as particle (grain) size and crystallinity. Aside from instrumental factors, the greatest contribution to the peak shape is frequently due to crystallite size. The Bragg law (Eq. 3.3) is only completely valid

when the crystallite size is essentially infinite; for a crystallite of a finite size the diffracted intensity of the Bragg peak will spread over a region, where the size and peak shape are related to the crystallite size and shape. The degree of Bragg peak broadening due to the sample can be used to estimate the crystallite size using relationships, such as the Scherrer equation, given by [20, 21];

$$t = \frac{k \times \lambda}{\beta \times \cos\theta} \qquad \text{---------- (3.4)}$$

Where, t is the sub structure/grain size, λ is the wave length of X–ray source (~ 1.5406 Å), k is the constant varying from 0.844 to 0.99, depending on type of lattice, θ is the angle of diffraction of a chosen XRD peak, β is the $[(\beta_M)^2 - (\beta_S)^2]^{½}$, β_M is the full width at half maximum of XRD peak and β_S is the full width at half maximum of XRD peak of standard large grained material (grain size 50 μm).

3.4 Hydriding – Dehydriding Analysis Using Sievert's Equipment

To characterize a potential hydrogen storage material, it must measure the amount of hydrogen it absorbs at various temperatures and pressures. The absorption amount is typically measured as a function of pressure, while the temperature is held constant. The experimental apparatus (Sievert's equipment) is working based on that principle, known as "Sievert's principle" [22, 23]. Volumetric high pressure hydrogen absorption/desorption measurements have been carried out using in-house built volumetric apparatus. A schematic P & ID (Process and Instrumental Diagram) of the apparatus used for experimental work is shown in Fig. 3.8 [24, 25].

The experimental apparatus consists of (see Fig. 3.9):

- A cylindrical sample holder or hydriding reactor of known volume, 11 cm^3
- A furnace (maximum temperature range up to 500 °C)
- A hydrogen reservoir of known volume, 270.45 cm^3
- A pressure transducer or sensor of about 0 to 100 bar (accuracy 0.01% of full scale) to measure pressure of the system
- A high vacuum system with rotary and diffusion pump set up

- A pirani gauge with gauge head to measure vacuum pressure in the range 0 to 10^{-3} bar for rotary pump
- A penning gauge with gauge head to measure vacuum pressure in the range 10^{-3} to 10^{-7} bar for diffusion pump
- "K" type thermocouples (Cr–Al type) (sensitivity 1 °C) to measure the temperature of the reactor
- Four needle valves (SS–316) with pressure sustainability up to 70 kg/cm^2 of hydrogen
- Hydrogen cylinder with capacity of 150 kg/cm^2 of hydrogen

Using this system pressure up to 10 MPa can be achieved. All components are made of stainless steel (SS–316). High pressure needle valves are used in the gas line for controlling the gas flow. All possible sources of leakage are carefully inspected. Care has been taken to avoid the errors due to factors such as temperature instability, leaks and additional pressure and temperature effects caused by expanding the hydrogen from the reservoir to reactor.

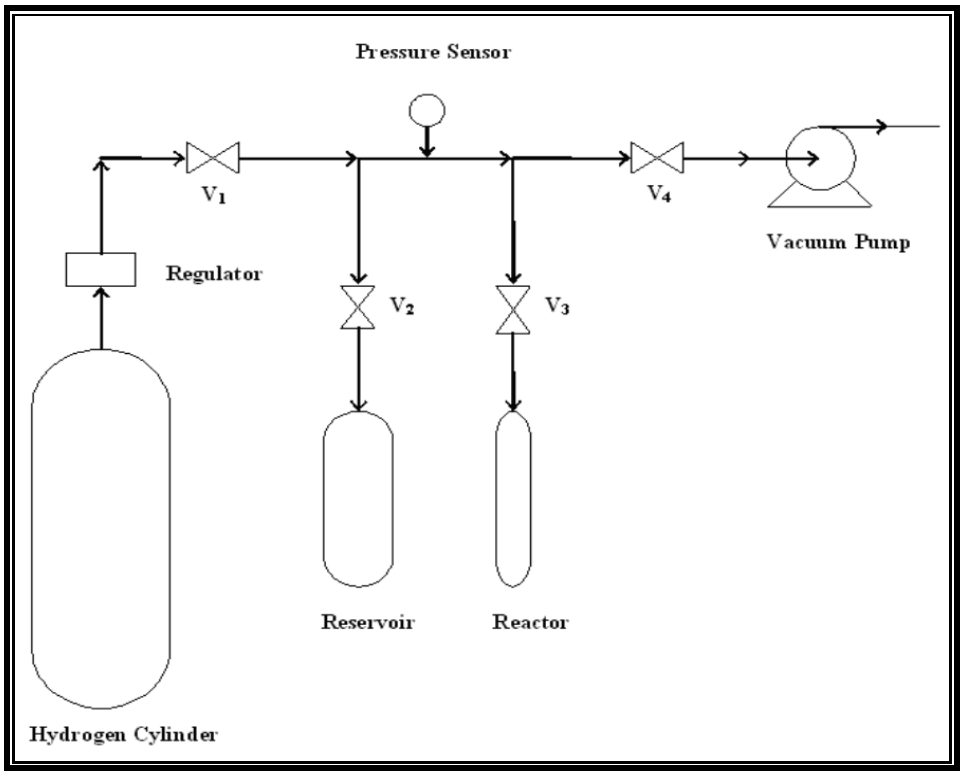

Fig. 3.8: P & ID Diagram of hydrogen absorption and desorption apparatus used for the experimental work

Fig. 3.9: Photograph showing experimental setup of hydrogen absorption and desorption apparatus

The laboratory experimental work of absorption and desorption is divide into three parts, namely, (i) Vacuum procedure, (ii) Computation of absorbed mass% of hydrogen and (iii) Computation of desorbed mass% of hydrogen. A brief explanation of each part is given as under:

3.4.1 Vacuum Procedure

To minimise oxygen contamination during charging/discharging of hydrogen, whole hydrogen absorption/desorption chamber evacuate less than 10^{-6} bar using high vacuum pump system. This was done by combine rotary and diffusion pump systems (make by Hind High Vacuum Co. (P) Ltd., Banglore, India, Model no. 12A 4). To create high vacuum, the simple process steps are given as under:

- Start the water flow.
- Switch on the main units.
- Open the "Roughing valve "and allow the vacuum to achieve 10^{-3} bar on the vacuum gauge.

- Open the “Backing valve “and wait 2 minute.
- Close the “Roughing valve “and wait 15 minute.
- Switch on the diffusion pump and wait 10 minute.
- Open the “Baffle valve “and wait the vacuum achieved less than 10^{-4} bar.

3.4.2 Computation of the Absorbed Mass% of Hydrogen

To compute absorbed mass percent of hydrogen into synthesized metal alloys/compositions, the following steps are done using in-house developed experimental set up:

- ☼ Measure the weight of sample, which was used to study for the hydrogen storage capacity characterization (0.5 gm to 1.0 gm).
- ☼ Keeping sample powder in reactor and create leak proof charging chamber.
- ☼ Close valve V_1.
- ☼ Open valves V_3 (reactor valve) and V_4 (vacuum valve) for evacuation.
- ☼ Switch on the rotary pump and evacuate up to 0.2×10^{-3} bar.
- ☼ Switch on the diffusion pump to evacuate less than 10^{-4} bar.
- ☼ Close valve V_3 and V_4.
- ☼ Switch off the diffusion pump and after half an hour, switch off the rotary pump.
- ☼ Open the valve V_1 and supply pure hydrogen (minimum 99.99% with Grade – I) up to 30 bar.
- ☼ Switch on the heater and heat for charging temperature up to 200 ºC.
- ☼ Open the valve V_3 (reactor valve).
- ☼ Note down the pressure at one minute time interval until the pressure is constant.
- ☼ Remove the heater and cool up to room temperature (using Fan).

The amount of hydrogen uptake into the synthesized alloys/compositions is calculated from the pressure drop in a known volume using the ideal gas law.

Let, V_a be the volume of reaction chamber without reactor connected, then the V_a is measured as:

$$V_a = V_R + V_p \qquad \text{---------- (3.5)}$$

Where, V_R is the volume of reservoier ($\approx 285.45 \times 10^{-6}$ m^3) and V_p is the volume of connected pipelines between valves V_2 and V_3 ($\approx 25.0 \times 10^{-6}$ m^3).

Therefore, the number of moles in reaction chamber before charging, n_1 is calculated as:

$$n_1 = \frac{P_1 \times V_a}{R \times T_1} \quad \text{---------- (3.6)}$$

Where, P_1 is the initial pressure (before charging), T_1 is the room temperature and R is the gas constant.

And, the number of moles in a reaction chamber after charging, n_2 is calculated as:

$$n_2 = \frac{P_2}{R}\left[\frac{V_a + V_{pr}}{T_1} + \frac{V_r}{T_2}\right] \quad \text{---------- (3.7)}$$

Where, P_2 is the final pressure (after charging), V_{pr} is the volume of connected pipeline between valve V_3 and rector ($\approx 7.3 \times 10^{-6}$ m^3), V_r is the volume of reactor ($\approx 11.5 \times 10^{-6}$ m^3) and T_2 is the charging temperature.

Therefore, the number of absorbed moles during charging process, n is,

$$n = n_1 - n_2 \quad \text{---------- (3.8)}$$

$\therefore$ The mass of absorbed hydrogen into the synthesized materials is,

$$m = 2 \times n \quad \text{---------- (3.9)}$$

Hence, the mass% of absorbed hydrogen in the synthesized alloys/compositions is computed as:

$$Mass\% = \frac{m}{m+M} \times 100\% \quad \text{---------- (3.10)}$$

Where, M is the mass of synthesized alloy composition.

3.4.3 Computation of the Desorbed Mass% of Hydrogen

To compute desorbed mass% of hydrogen into synthesized alloys/compositions, the following steps are done using in-house developed experimental set up:

- ☼ Open valve V_4 to vent hydrogen into air, and closed it, when hydrogen pressure nearly 0.1 bar.
- ☼ Close valves V_2, V_3 and V_4.
- ☼ Switch on the heater to achieve the required discharging temperature (≈ 350 ºC).
- ☼ Open valve V_3.
- ☼ Note down chamber pressure in regular time interval until pressure is constant.

The amount of hydrogen release from the synthesized alloys/compositions is also calculated as per the absorption.

The number of moles in reaction chamber before discharging, n_1 is calculated as:

$$n_1 = \frac{P_1 \times \left(V_p + V_{pr} + V_r\right)}{R \times T_1} \quad \text{---------- (3.11)}$$

Where, P_1 is the initial pressure (before discharging).

And, the number of moles in reaction chamber after discharging, n_2 is calculated as:

$$n_2 = \frac{P_2}{R}\left[\frac{V_p + V_{pr}}{T_1} + \frac{V_r}{T_2}\right] \quad \text{---------- (3.12)}$$

Where, P_2 is the final pressure (after discharging) and T_2 is the discharging temperature.

Therefore, the number of desorbed moles of hydrogen during discharging process, n is computed as:

$$n = n_2 - n_1 \qquad \text{---------- (3.13)}$$

The mass of desorbed hydrogen from the synthesized alloys/compositions is calculated as:

$$m = 2 \times n \qquad \text{---------- (3.14)}$$

Hence, the mass% of desorbed hydrogen from the synthesized alloys/compositions is computed as per Eq. (3.10).

3.5 Thermal Analysis – Differential Scanning Calorimetry (DSC)

Differential Scanning Calorimetry (DSC) is the calorimetric measurement of the exothermic and endothermic processes occurring upon the controlled heating and cooling rate on a sample [26, 27]. Useful information on the temperature and enthalpy of phase transitions such as melting, crystallization and reactions can be obtained from this technique (see Fig. 3.10). DSC involves the measurement of the change of the difference in the rate of heat flow (power) to/from a sample relative to a reference sample, when both are subjected to the same temperature program regime. The principles involved in a DSC measurement share many similarities to DTA (differential thermal analysis) experiment [28, 29]. DSC measurement, it is the heat flow to/from the sample (and reference) which is recorded. As such, this has a much more direct relation to the enthalpy of the thermal event being observed. The exchange of heat to the sample (and reference) mainly takes place via a well defined pathway, through a material with a known thermal resistance. The temperature of this conduction pathway is monitored for the sample and the reference and the temperature difference between the two is proportional to the difference in heat flow

rates for the sample and reference. A schematic of a typical heat flow DSC experimental setup is shown in Fig. 3.11.

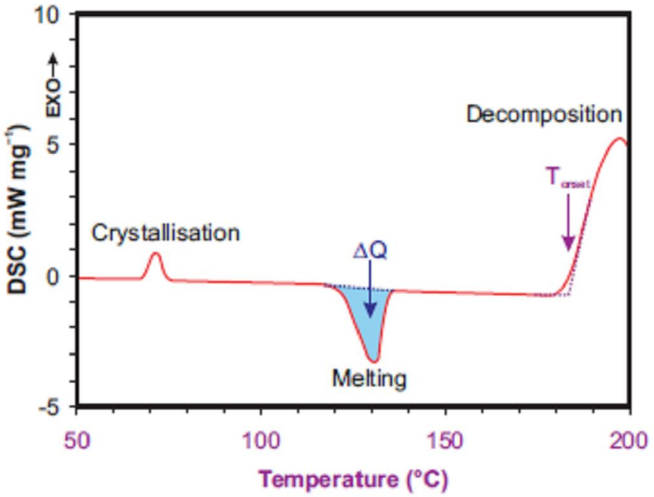

Fig. 3.10: Example of a typical DSC trace

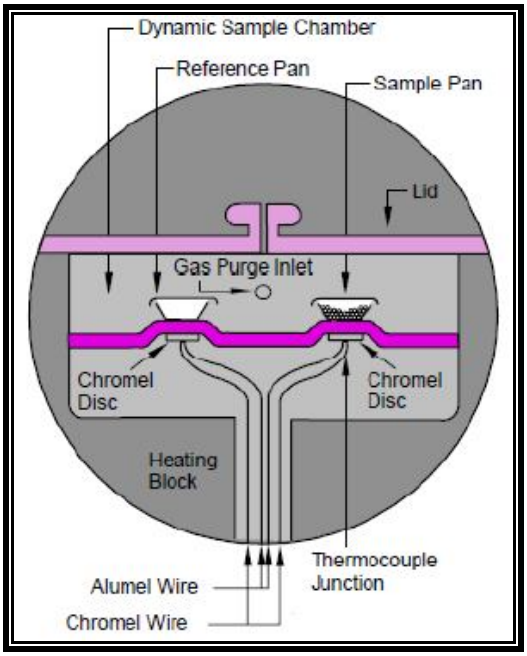

Fig. 3.11: Schematic diagram of the experimental DSC setup

Laboratory DSC

DSC measurements are performed on a calibrated DSC 822 METTLER TOLEDO (see Fig. 3.12). Sample of approximately 10 mg is loaded into a shallow Al pan. The reference is used an empty Al sample pan. A constant atmosphere of 3 to 5 bar of Nitrogen (99.998% pure with Grade–I) was achieved inside the DSC at a flow rate of 100 ml min^{-1} for the minimizing oxygen contamination. Typical experiments involved a ramp at 5 °C min^{-1} up to 400 °C.

Fig. 3.12: Photograph showing the laboratory differential scanning calorimetry (DSC)

Based on an integration of the differential power with respect to time, the net heat liberated, ΔQ, which is numerically equal to enthalpy change, is obtained as:

$$\Delta Q \equiv \int_{t_{start}=0}^{t_{end}} (\Delta P)dt = \Delta H \qquad \text{---------- (3.15)}$$

Where, ΔP is the differential power and t is the time.

The above enthalpy is converted to specific enthalpy, $\overline{\Delta H}$ by:

$$\overline{\Delta H} = \int_0^{t_{end}} \frac{(\Delta P)}{m} dt \qquad \text{---------- (3.16)}$$

Further, if one assumes the dehydriding reaction in the DSC to be close to equilibrium (which is thermodynamically unlike), "pseudo specific entropy", $\overline{\Delta S_{pseudo}}$ can compute as:

$$\overline{\Delta S_{Pseudo}} = \int_0^{t_{end}} \frac{(\Delta P)}{m\ T(t)} dt \qquad \text{---------- (3.17)}$$

Where, $T = \alpha t$ and α is the ramp rate.

REFERENCES

1. C. Suryanarayana, Mechanical alloying and milling, *Progress in Materials Science*, 46 (2001) 1–184.
2. L. Lu and M. O. Lai, Mechanical Alloying, *Kluwer Academic Publishers*, Boston/Dordrecht/London (1998) 13–18.
3. M. Abdellaoui and E. Gaffet, *Journal De Physique IV*, **4** (1994) 291–296.
4. http://en.wikipedia.org/wiki/Scanning_electron_microscope
5. www.serc.carleton.edu/research_education/geochemsheets/techniques/SEM.html
6. A. Bogner, P. H. Jouneau, G. Thollet, D. Basset and C. Gauthier, *Micron*, **38** (2007) 390–401.
7. www.web.utk.edu/~prack/MSE%20300/SEM.pdf
8. B. Voutou and E. Stefanaki, Electron Microscopy: The Basics, *Physics of Advanced Materials Winter School* (2008).
9. www.mtse.unt.edu/FAULTY/bgorman/30201
10. B. Hafner, Energy Dispersive Spectroscopy on the SEM: A Primer, Characterization Facility, University of Minnesota—Twin Cities.
11. www.en.wikipedia.org/wiki/Energy-dispersive_X-ray_Spectroscopy
12. V. K. Pecharsky and P. Y. Zavalij, Fundamentals of Powder Diffraction and Structural Characterization of Materials, *Library of Congress Cataloging-in-Publication Data, Springer* (2005) 138–146.
13. J. P. Glusker, m. Lewis and M. Rossi, Crystal Structure Analysis for Chemists and Biologists, *VCH press* (1994) 74 – 79.
14. B. D. Cullity, Elements of X – Ray Diffraction, *Addison-Wesley Publishing Company, INC. Reading, Massachusetts* (1956) 78 – 85.
15. G. S. Rohrer, Structure and Bonding in Crystalline Materials, *Cambridge University Press* (2004) 205–206.
16. L. V. Azaroff and M. J. Buerger, The Powder Method in X–Ray Crystallography, *McGRAW – Hill Book Company, Inc., New York, Toronto and London* (1958) 4–11.
17. B. B. He, Two – Dimensional X – Ray Diffraction, *A John Wiley & Sons, Inc., Publication* (2009) 13–14.
18. P. A. Chater, Mixed Anion Complex Hydrides for Hydrogen Storage, *Dissertation of Doctoral, University of Birmingham* (2009) 26–41.

19. D8 X–Ray diffractometer, *User's Manual Vol. I* (2005) 2–1 to 2–41.
20. M. Abdellaoui, D. Cracco and A. Percheron-Guegan, *J. of Alloys and Compounds,* **268** (1998) 233–240.
21. C. Suryanarayana and M. Grant Norton, X – Ray Diffraction – Practical approach, *Plenum Press, New York and London* (1998) 207 – 214.
22. K. B. Gerasimov, I. G. Konstanchuck, S. A. Chizhik and J. L. Bobet, *Int. J. of Hydrogen Energy*, **34** (2009) 1916 – 1921.
23. G. Liang, *J. of Alloys and Compounds, xxx (2004) xxx–xxx (article in press)*.
24. Q. Li, K. C. Chou, Q. Lin, L. J. Jiang and Feng Zhan, *Int. J. of Hydrogen Energy*, **29** (2004) 843–849.
25. J. Kapischke and J. Hapke, *Experimental Thermal and Fluid Science*, **18** (1998) 70–81.
26. P. Gabbott, Principles and Applications of Thermal Analysis, *Blackwell publishing* (2007) 2–49.
27. www.usercom1/2000//METTER TOLEDO thermal analysis systems
28. P. K. Gallagher, Handbook of Thermal Analysis and Calorimetry, *Elsevier publisher* (2003) 7–21.
29. P. J. Haines, Principles of Thermal Analysis and Calorimetry, *RSC Royal Society of Chemistry* (2002) 166–187.